Delayed Onset of Nonthermal Melting in Single-Crystal Silicon Pumped with Hard X Rays

T. Pardini, J. Alameda, A. Aquila, S. Boutet, T. Decker, A. E. Gleason, S. Guillet, P. Hamilton, M. Hayes, R. Hill, J. Koglin, B. Kozioziemski, J. Robinson, K. Sokolowski-Tinten, R. Soufli, and S. P. Hau-Riege

Phys. Rev. Lett. **120**, 265701 — Published 25 June 2018

DOI: 10.1103/PhysRevLett.120.265701

Delayed onset of non-thermal melting in single-crystal silicon pumped with hard X-rays

T. Pardini,[1,*] J. Alameda,[1] A. Aquila,[2] S. Boutet,[2] T. Decker,[1] A. E. Gleason,[3] S. Guillet,[2] P. Hamilton,[1] M. Hayes,[2] R. Hill,[1] J. Koglin,[2] B. Kozioziemski,[1] J. Robinson,[1] K. Sokolowski-Tinten,[4] R. Soufli,[1] and S. P. Hau-Riege[1]

[1] *Lawrence Livermore National Laboratory, 7000 East Ave., Livermore, CA 94550*
[2] *SLAC National Accelerator Laboratory, Menlo Park, CA 94025 USA*
[3] *Shock and Detonation Physics, Los Alamos National Laboratory, P.O. Box 1663, Los Alamos, New Mexico 87545, USA*
[4] *Faculty of Physics and Center for Nanointegration Duisburg-Essen (CENIDE), University of Duisburg-Essen, Lotharstrasse 1, 47048 Duisburg, Germany*

In this work we monitor the onset of non-thermal melting in single-crystal silicon by implementing an x-ray pump/x-ray probe scheme. Using the ultra-short pulses provided by the Linac Coherent Light Source (LCLS, SLAC), and a custom-built split-and-delay line for hard x-rays, we achieve the temporal resolution needed to detect the onset of the transition. Our data shows no loss of long range order up to 150 ± 40 fs from photo-absorption, which we interpret as the time needed for the electronic system to equilibrate at or above the critical non-thermal melting temperature. Once such equilibration is reached, the loss of long range atomic order proceeds inertially, and is completed within 315 ± 40 fs from photo-absorption.

INTRODUCTION

The ultra-fast loss of atomic periodicity in a crystal following the absorption of a high fluence photon pulse is a remarkable effect. It has been experimentally observed to date in a number of covalently bonded materials [1–7] exposed to high-fluence lasers at infra-red wavelengths. It is well understood [8–18] that ultra-fast melting is triggered by the excitation of a large number of electrons into the conduction band. Electronic thermalization above some threshold temperature causes a significant number of bonding states to be depleted and anti-bonding states to be populated. Then, ions experience a significant change in the electrostatic potential leading to inertial displacement from their equilibrium positions. Recoules [8] and co-workers found numerically that a threshold electronic temperature of 1.5 eV/atom is enough to cause an ultra-fast lattice instability in silicon. This instability is named non-thermal melting due to the lack of thermal equilibration between the electronic and ionic systems. To date, experiments investigating non-thermal melting in semiconductors have implemented a laser-pump/laser-probe or a laser-pump/x-ray probe approach. In all cases, a laser pump with a pulse length ranging between 50 and 120 fs is tuned to optical wavelengths, and directly excites valence electrons to the conduction band. The low-energy nature of the photo-electrons generated this way leads to a fast equilibration above the threshold temperature, with a time scale that is negligible compared to the duration of the melting transition. As a result, the consistent picture emerging from the data is that of a solid-to-liquid transition which completes on a sub-picosecond time scale with a nearly instantaneous onset. It is reasonable to ask how the time scale for the onset of non-thermal melting would be affected by pumping the system with hard x-rays. In this case, photo-absorption would be dominated by core-level electrons, leading to fast photo-electrons. Electron equilibration above the threshold temperature would proceed via secondary electron cascading with a time scale of up to 60 fs [19], delaying the onset of non-thermal melting. The measurement of such delay is the subject of this work.

The advent of X-ray Free Electron Lasers (XFELs) has enabled the production of ultra-short x-ray pulses with fluences in the kJ/cm^2 range. The LCLS [20], is capable of producing such pulses up to hard x-ray energies. At the Lawrence Livermore National Laboratory (LLNL), in collaboration with LCLS, we have developed an x-ray split-and-delay line named MEL-X (Mirror-based dElay Line for X-rays) [21]. The deployment of the MEL-X at the LCLS has enabled a new category of experiments related to ultra-fast melting in semiconductors, characterized by an x-ray pump/x-ray probe scheme. The advantages of such a scheme are: (i) the x-ray nature of the pump beam allows us to investigate the effect of core-level excitations on the time scale of non-thermal melting; (ii) the x-ray nature of the probe beam offers a direct structural probe via Bragg diffraction; (iii) the short pulse length (pump and probe) of the LCLS provides the necessary resolution to detect the onset of the transition; (iv) the high intensity of the MEL-X pump beam allows us to reach pump doses relevant to non-thermal melting Physics. Using silicon as our test case, we pump the crystal with 5.95 keV x-ray pulses at a peak fluence of nearly 9 eV/atom (4 eV/atom average), well above the damage threshold. At this photon energy, the absorption cross section of valence electrons is negligible, and the depletion of bonding states cannot begin at the photo-absorption stage since it is dominated by core-electrons. The large number of down-scattering events necessary to thermalize the primary electrons sets the

time scale of the cascading effect, and therefore of the bonding states depletion. We then directly probe the structural response of the excited material by monitoring the Si(333) Bragg reflection at 5.95 keV, with pump-probe delays in the 100 - 400 fs range. Our data shows no measurable change in crystal order within 150 ± 40 fs from photo-absorption. We argue that such delayed onset is due to the time it takes the secondary electron cascade to complete, in agreement with the calculations of Medvedev and co-workers [17]. Once the electronic system is thermalized, ions are displaced inertially from their equilibrium positions in agreement with previous results [3], and a complete loss of reflectivity is measured within 315 ± 40 fs.

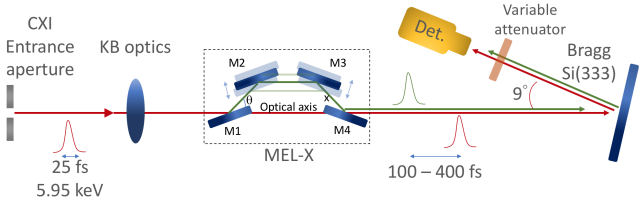

FIG. 1. A schematic view of the experimental set-up. A 25 fs FWHM pulse from the LCLS is split into a pump and probe beam by the MEL-X, which is installed ∼ 4 meters downstream of the focusing optics, and ∼ 4 meters upstream of the sample plane. The Si(333) Bragg reflection is measured in near back-scattering geometry on a pixel array detector [22]. The insertion depth error of the M2 and M3 MEL-X mirrors with respect to the optical axis is schematically shown in the figure, and represents the most significant source of uncertainty for the pump-probe delay.

The data presented in this work was collected at the Coherent X-ray Imaging (CXI) instrument at LCLS [23]. Figure 1 shows a schematic of the experimental set-up. Details on the MEL-X engineering have been provided elsewhere [21]. Its design includes four x-ray mirrors working at a grazing angle of 0.5 degrees. Each x-ray mirror is coated with 300 Å of iridium, yielding 79% reflectivity at 5.95 keV. The LCLS was operated in SASE mode, with an average pulse energy of 2.4 mJ, and a photon energy of 5.95 keV. The length of the pump and probe pulses was 25 fs. A spectrometer deployed in parasitic mode measured the spectral content of each x-ray pulse. Attenuators upstream of the sample were used to lower the x-ray pump dose. These, combined with the beamline and MEL-X transmission, and the spectrometer absorption, yielded an overall pump transmission of the experimental set-up equal to 1%. The Si(333) Bragg reflection was measured on a pixel array detector [22] in near back-scattering geometry. A 200 μm-thick silicon single-crystal attenuator with variable transmission was placed between the sample and the detector to limit the number of photons to within the dynamic range of the latter. The detector output was normalized by the spectrometer calibrated output. The sample consisted of silicon pillars etched in a 1 mm-thick Si(111) wafer. Details on the sample engineering have been given elsewhere [24]. The pump-probe delay (Δt) was determined by geometric considerations during off-line alignment of the MEL-X. In the ideal case of a perfectly aligned MEL-X, $\Delta t = 2x(1 - \cos(2\theta))$, where x is the M1-to-M2 and M3-to-M4 mirror separation along the probe beam axis, and θ is the grazing incidence angle on M1. Errors in mirror alignment translated in an overall uncertainty on the pump-probe delay of ± 40 fs. This value represents the largest possible error (max-min), and it is mostly caused by the insertion depth error of the M2 and M3 mirrors with respect to the optical axis, resulting in M2 and M3 intercepting the x-ray beam sooner or later than nominal, affecting the path length difference. The overlap between the pump and probe beam was checked and optimized before every data set, using a high resolution microscope imaging the fluorescence off a YAG screen at the sample plane, and implementing a centroid method to achieve the necessary spatial resolution. We collected data at four delay times: 150 fs, 220 fs, 315 fs, and 385 fs. For each delay investigated, data was collected in two modes: with pump and probe beams separated by 50 μm at the focal plane, and with pump and probe beams overlapped at the focal plane. In both modes, the integrated signal from pump and probe was simultaneously measured on the detector. For the non-overlapped mode, given that the beams hit different spots on the sample, the integrated detector signal ($I_0 = I_0^{pp} + I_0^{pr}$) is proportional to the unperturbed silicon single-crystal reflectivity, independent of delay time. On the contrary, for the overlapped mode, the integrated detector signal ($I = I^{pp} + I^{pr}$) allows us to extract the probe reflectivity as a function of delay, once the relative intensity of the pump and probe beams is known. To this end, we have performed a detailed characterization of both beam intensity profiles at the focal plane.

Beam imprints (not shown here) were obtained by exposing a 400 Å-thick gold film deposited on glass to focused x-ray pulses at different values of fluence. The size of the imprints was measured with a Scanning Electron Microscope (SEM). Following Liu's method [25], we estimate $\sigma_x^{pp} = 2.20 \pm 0.06$ μm, $\sigma_y^{pp} = 0.76 \pm 0.06$ μm for the pump beam, and $\sigma_x^{pr} = 2.20 \pm 0.05$ μm, $\sigma_y^{pr} = 0.83 \pm 0.02$ μm for the probe beam. We then implement numerical wavefront propagation simulations to estimate the one- and two-dimensional beam intensity profiles at the focal plane [26–28], shown in Figure 2(a). The elongated nature of the intensity profile along the x-axis is due to edge diffraction off the MEL-X beam splitter. Our simulations yield $\sigma_x^{pp} = 2.1 \pm 0.03$ μm and $\sigma_y^{pp} = 0.74 \pm 0.03$ μm, in excellent agreement with the imprint analysis. From the numerical results we estimate the dose at the sample imparted by the pump beam, shown in the color scale of the intensity map. We as-

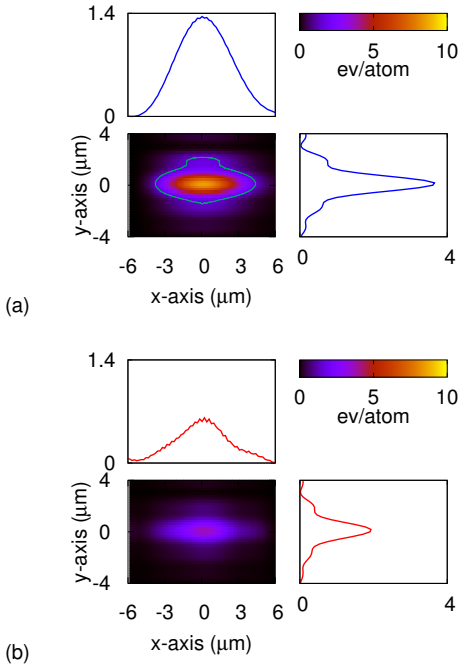

FIG. 2. Simulated intensity profile for the pump (a) and probe (b) beam at the sample location. The contour line in (a) represents the 1.5 eV/atom contour. 65% of the pump intensity is contained within this contour. The intensity of the probe beam has been scaled by a factor of 0.4 to account for the four-bounce reflectivity of the MEL-X along the probe beam path

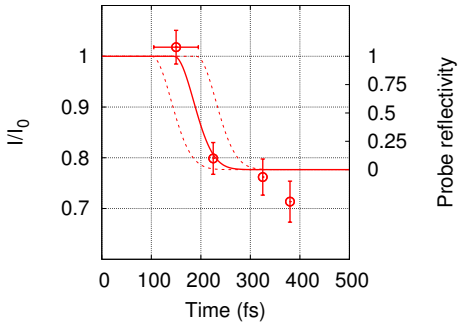

FIG. 3. The ratio $\frac{I}{I_0}$ of the Bragg signal at the detector as a function of the delay times (red circles). The right y-axis shows the probe reflectivity. The theoretical loss of reflectivity as a function of time assuming an inertial model is shown with a solid red line. Dash lines represent the temporal uncertainty.

sume a 30μm attenuation length for silicon at 5.95 keV. We conclude that 35% of the pump intensity lays outside the threshold energy region of 1.5eV/atom indicated by the contour line in the 2D plot. The numerically simulated probe beam intensity profile is shown in Figure 2(b), from which we derived $\sigma_x^{pr} = 2.0 \pm 0.04$ μm and $\sigma_y^{pr} = 0.76 \pm 0.04$ μm, in reasonable agreement with imprint analysis.

The numerically computed intensity profiles at the focal plane allow us to translate the integrated detector signal into the probe reflectivity measured as a function of delay time. While for no loss of crystal order we obviously expect $\frac{I}{I_0} = 1$, a complete loss of probe reflectivity would yield $\frac{I}{I_0} = \frac{I^{pp}+CI^{pr}}{I_0^{pp}+I_0^{pr}} = 0.77$. Here I^{pp} and I^{pr} are the integrated pump and probe intensities obtained from our numerical simulations, and $C = 0.35$ accounts for the 35% of the probe intensity reflecting off unperturbed silicon.

Figure 3 shows the $\frac{I}{I_0}$ signal measured at the four delay times investigated. The right y-axis shows the corresponding probe reflectivity. Temporal error bars are shown for the t=150 fs data point only. In fact, while the initial position uncertainty on M2 and M3 caused an absolute $\pm$ 40 fs uncertainty, the relative uncertainty among different delay times is negligible given that the two mirrors are moved with micrometer precision. From the data we draw the following conclusions. No sign of atomic motion is detected within 150 $\pm$ 40 fs from photo-absorption. At 220 $\pm$ 40 fs, the probe Bragg signal has dropped to $\sim$12%. Finally, after 315 $\pm$ 40 fs no probe Bragg reflectivity is observed, indicating a complete loss of long range atomic order. In agreement with Lindenberg and co-workers [3], we assume that the loss of atomic long range order is inertial in nature. Prior to photo-absorption, ions are oscillating about their equilibrium positions with kinetic energy $\frac{1}{2}mv_{rms}^2 = \frac{3}{2}k_BT$, where m is the silicon atomic mass, v_{rms} is the atomic root-mean-square velocity, k_B is the Boltzmann constant, and $T = 300K$. After photo-absorption, and after the electronic system equilibrates at or above the threshold temperature of 1.5 eV/atom, the elastic potential bounding the ions at their equilibrium positions vanishes. Assuming inertial motion, the time-dependence of the reflectivity loss is given by the Debey-Waller factor as $R(t) = \exp[-q^2v_{rms}^2(t-t_0)^2]$. Here $q^2 = \frac{2\pi}{d}$, where d is the lattice constant of the Si(333) crystal orientation. A plot of the computed probe reflectivity as a function of time is shown with a solid line in figure 3. The curve has been fitted to the data with the only degree of freedom being the temporal onset of the transition (t_0), which we find to be 150 $\pm$ 40 fs. Ultimately, we conclude that for silicon pumped with hard x-rays $t_0 \geq 110$ fs. We argue that this result must be valid for pump doses relevant to non-thermal melting Physics, i.e. a few times above the damage threshold dose. Work done on biological samples [29], clusters [30], and fullerenes [31], shows atomic motion as soon as 30 fs from photo-excitation in some cases, but at pump doses up to three orders of magnitude above the damage threshold. Given the average pump dose imparted to our sample (4 eV/atom), we conclude that about 1 out 1000 atoms participate in photo-

absorption. Therefore, approximately 0.1% of the atoms will have a deep core-hole left behind, which is quickly filled during Auger production. This leads to the formation of a valence hole within 10 fs from excitations [19]. At this stage, no appreciable change in electrostatic potential is present, since only 0.1% of valence electrons have been perturbed, and most bonding states are still occupied. The absorbed pulse energy is stored in the high kinetic energy of the photo-electrons which begin down-scattering with neighboring valence electrons. This initiates the cascading effect, which excites more valence electrons into the conduction band. A time-independent estimate based on a free electron model at the average absorbed x-ray dose of 4 eV/atom, suggests that in our experiment approximately 15% of the valence electrons are excited to the conduction band. This is well beyond the 10% value above which non-thermal melting is believed to take place. Medvedev and co-workers [19] showed that, in SiO_2 excited by a 7 keV pulse, the maximum electron density in the conduction band is reached approximately 60 fs after photo-excitation, as each primary electron must undergo over four hundred collisions. Interestingly, the same time scale ($\sim$ 50 fs) is found by the same authors for silicon pumped by 1 keV x-ray pulses [17]. In the latter work, the authors also compute the time scale for the onset of atomic motion after photo-absorption. They show that atoms gain appreciable kinetic energy approximately 100 fs after photo-absorption, nearly 50 fs after the anti-bonding states have experienced their maximum population. We claim that our data capturing the onset of non-thermal melting in silicon at 6 keV is consistent with this picture. Experimentally we set a lower limit for the onset of atomic motion measuring 110 fs, which we interpret according to Medvedev's results as the time needed to thermalize the electronic system and modify appreciably the potential landscape to trigger atomic displacement.

In conclusion, we have studied non-thermal melting in single-crystal silicon pumped with 5.95 keV x-ray pulses. Our data suggests that for silicon pumped with hard x-rays at least 110 fs are needed for the electrons to thermalize at or above the threshold temperature of 1.5 eV/atom. We argue that this rather long time scale is caused by the several hundred collisions necessary to thermalize the fast photoelectrons. Once the transition begins, ions are displaced inertially from their equilibrium positions, and within 315 $\pm$ 40 fs no long range order exists, as evidenced by the lack of probe reflectivity.

We thank Dr. Daniele Cocco and his group for their help with the MEL-X substrates metrology. This work was performed under the auspices of the U.S. Department of Energy by Lawrence Livermore National Laboratory under Contract DE-AC52-07NA27344. This work was funded by the Laboratory Directed Research and Development Program at LLNL. KST acknowledges support by the "Deutsche Forschungsgemeinschaft" through the Collaborative Research Center 1242 "Non-Equilibrium Dynamics of Condensed Matter in the Time Domain. Los Alamos National Laboratory is operated for the U.S. DOE National Nuclear Security Administration under contract DE-AC52-06NA25396. Use of the Linac Coherent Light Source (LCLS), SLAC National Accelerator Laboratory, is supported by the U.S. Department of Energy, Office of Science, Office of Basic Energy Sciences under Contract No. DE-AC02-76SF00515. Document Release Number LLNL-JRNL-740585.

* pardini2@llnl.gov

[1] k. Sokolowski-Tinten, J. Bialkowski, and D. Vonderlinde, Phys. Rev. B **51**, 14186 (1995).
[2] A. Rousse *et al.*, Nature **410**, 65 (2001).
[3] A. Lindenberg *et al.*, Science **308**, 392 (2005).
[4] K. Gaffney *et al.*, Phys. Rev. Lett. **95** (2005).
[5] P. B. Hillyard *et al.*, Phys. Rev. Lett. **98** (2007).
[6] C. Siders *et al.*, Science **286**, 1340 (1999).
[7] G. Sciaini *et al.*, Nature **458**, 56 (2009).
[8] V. Recoules, J. Clerouin, G. Zerah, P. Anglade, and S. Mazevet, Phys. Rev. Lett. **96** (2006).
[9] Y. Izawa, S. Tokita, M. Hashida, M. Fujita, and Y. Izawa, Review of Laser Engineering **34**, 773 (2006).
[10] P. B. Hillyard, D. A. Reis, and K. J. Gaffney, Phys. Rev. B **77** (2008).
[11] W. Marine, N. Bulgakova, L. Patrone, and I. Ozerov, App. Phys. A **79**, 771 (2004).
[12] P. Silvestrelli, A. Alavi, M. Parrinello, and D. Frenkel, Phys. Rev. Lett. **77**, 3149 (1996).
[13] P. Stampfli and K. Bennemann, App. Phys. A **60**, 191 (1995).
[14] C. V. Shank, R. Yen, and C. Hirlimann, Phys. Rev. Lett. **51**, 900 (1983).
[15] S. Sundaram and E. Mazur, Nat. Mat. **1**, 217 (2002).
[16] D. P. Korfiatis, K.-A. T. Thoma, and J. C. Vardaxoglou, J. Phys. D **40**, 6803 (2007).
[17] N. Medvedev, Z. Li, and B. Ziaja, Phys. Rev. B **91** (2015), 10.1103/PhysRevB.91.054113.
[18] S. Feng, J. Zhao, X. Cheng, and H. Zhang, J. Appl. Phys. **114**, 043519 (2013).
[19] N. Medvedev, B. Ziaja, M. Cammarata, M. Harmand, and S. Toleikis, Cont. Plasma Phys. **53**, 347 (2013).
[20] C. Bostedt *et al.*, Rev. Mod. Phys. **88** (2016).
[21] T. Pardini *et al.*, Proc. SPIE **9589**, 95890T (2015).
[22] A. Dragone *et al.*, J. Phys. **493**, 012012 (2014).
[23] M. Liang *et al.*, J. Sync. Rad. **22**, 514 (2015).
[24] T. Pardini *et al.*, Phys. Rev. App. **1** (2014).
[25] J. Liu, Opt. Lett. **7**, 196 (1982).
[26] T. Pardini, D. Cocco, and S. P. Hau-Riege, Opt. Exp. **23**, 31889 (2015).
[27] T. Pardini, A. Aquila, S. Boutet, D. Cocco, and S. P. Hau-Riege, J. Sync. Rad. **24**, 738 (2017).
[28] J. E. Krist, Proc. SPIE **6675**, 66750P (2007).
[29] A. Barty *et al.*, Nat. Photonics **6**, 35 (2012).
[30] G. Faigel, Z. Jurek, G. Oszlanyi, and M. Tegze, J. Alloys Compd. **401**, 86 (2005).
[31] N. Berrah *et al.*, J. Mod. Phys. **63**, 390 (2016).